Structure, magnetic and optical properties, and Hall effect of Co- and Fe-doped SnO_2 films

Hyun-Suk Kim, Lei Bi, G. F. Dionne,* and C. A. Ross†
Department of Materials Science and Engineering, Massachusetts Institute of Technology, Cambridge, Massachusetts 02139, USA

Han-Jong Paik
Department of Materials Science and Engineering, Korea Advanced Institute of Science and Technology, Daejeon, 305-701, Republic of Korea

(Received 14 March 2008; revised manuscript received 31 May 2008; published 26 June 2008)

Magnetically doped SnO_2 is a promising dilute magnetic semiconductor and may also be applicable in a variety of magneto-optical applications. Epitaxial films of $Sn_{1-x}Co_xO_2$ ($x \leq 0.2$) and $Sn_{1-x}Fe_xO_2$ ($x \leq 0.4$) were grown by pulsed-laser deposition on *R*-plane Al_2O_3 substrates. Structural, magnetic, and magnetotransport measurements consistently point to a source of magnetism within the host lattice rather than from an impurity phase. The films are strained and their magnetic anisotropy is consistent with the presence of substantial amounts of magnetoelastic high-spin Fe^{2+}, or high- or low-spin Co^{2+}. $Sn_{0.9}Co_{0.1}O_2$ films have a reasonably high Faraday rotation of 570°/cm, and the refractive index n and extinction coefficient k at 1550 nm wavelength are 1.957 and 0.0102, respectively.

DOI: 10.1103/PhysRevB.77.214436 PACS number(s): 78.20.Ls, 75.80.+q, 75.50.Pp, 85.70.Sq

I. INTRODUCTION

Dilute magnetic semiconductors (DMS), in which ferromagnetic behavior above room temperature is induced in nonmagnetic semiconductors by doping with magnetic transition-metal (TM) ions, are of great interest as potential semiconductor-compatible magnetic components for practical spintronics applications.[1–3] Another promising application of DMS is to utilize the Zeeman effect of the localized magnetic moments of the transition-metal ions in high concentrations to create Faraday rotation of linearly polarized light. For example, paramagnetic $Cd_{1-x}Mn_xTe$ ($x=0.2-0.24$) is a good candidate for magneto-optical devices operating in the wavelength range of 600–800 nm.[4] Recently, ferromagnetism above room temperature has been reported in SnO_2 heavily doped with Co or Fe.[5,6] Ogale *et al.*[5] described $Sn_{1-x}Co_xO_2$ ($x<0.3$), which exhibits ferromagnetism with a Curie temperature (T_C) as high as 650 K, and with a magnetic moment reported as ~7.5 μ_B/Co. Subsequently, Coey *et al.*[6] reported room-temperature ferromagnetism ($T_C \sim 610$ K) in $Sn_{0.86}Fe_{0.14}O_2$ with a moment of 1.8 μ_B/Fe. Because SnO_2 is an attractive optical material with a large optical band gap (~3.6 eV),[7] DMS based on SnO_2 could be useful for a variety of applications requiring combined magnetic and optical functionality. However, there has been no report of the magneto-optical properties of TM-doped SnO_2 at communication wavelengths. Furthermore, select TM ions in oxide hosts can introduce large magnetoelastic effects through spin-orbit-lattice interactions in an octahedral crystal field.[8–10]

In this study, we report on the structural, magnetic, and magneto-optical properties of epitaxial $Sn_{1-x}Co_xO_2$ ($x \leq 0.2$) and $Sn_{1-x}Fe_xO_2$ ($x \leq 0.4$) films fabricated by pulsed-laser deposition. Their magneto-optical properties were characterized using Faraday rotation and optical absorption at 1550 nm wavelength. The origin of the correlated magnetic, optical, and magneto-optical properties will be discussed.

II. EXPERIMENT METHODS

The $Sn_{1-x}Co_xO_2$ ($x=0$, 0.02, 0.04, 0.1, 0.2, and 0.3) and $Sn_{1-x}Fe_xO_2$ films ($x=0$, 0.1, 0.2, 0.3, and 0.4) were grown by pulsed-laser deposition (PLD) using ceramic targets. The targets were prepared using standard solid-state reaction techniques. Prescribed amounts of SnO_2, Fe_2O_3, and CoO powders were mixed and pressed into disks with a diameter of 1 in, which were sintered at 1150 °C for 24 h in air. The sintered targets were ablated by a KrF excimer laser (Lambda Physik LPX200) operating at a wavelength of 248 nm and 10 Hz. The substrate temperature, oxygen pressure, and laser energy density were 700 °C, 2×10^{-6} Torr, and 1.5 J/cm^2, respectively. The films were cooled in the same oxygen pressure as used during deposition at a rate of 10 °C/min.

A typical thickness of the films was 500 nm, measured by Tencor P-10 profilometer. In order to investigate the structure, both two-dimensional (2D) (Ref. 11) and conventional one-dimensional (1D) x-ray diffraction (XRD) measurements were carried out using a Bruker AXS D8 DISCOVER with GADDS (General Area Detector Diffraction System) and a RIGAKU RU300, respectively. The chemical composition of the films was characterized by wavelength dispersive spectroscopy (WDS). This showed that the Co and Fe contents in the films, given above, are about 1.6 times higher than those in the targets, which is attributed to evaporative loss of Sn.[5,6] X-ray photoelectron spectroscopy (XPS) was used to analyze the elemental valence states in $Sn_{1-x}Co_xO_2$ and $Sn_{1-x}Fe_xO_2$ films. The microstructure and roughness of the TM-doped SnO_2 films were investigated by high-resolution transmission electron microscopy (HRTEM) and atomic force microscopy (AFM). The magnetic properties were measured using a quantum design SQUID magnetometer and an ADE vibrating sample magnetometer (VSM). Electrical resistivity, carrier concentration, and Hall-effect measurements were carried out using van der Pauw geometry. The magneto-optical behavior was investigated by measuring the Faraday rotation of 1550 nm wavelength light passing perpendicular to the film plane with the applied field

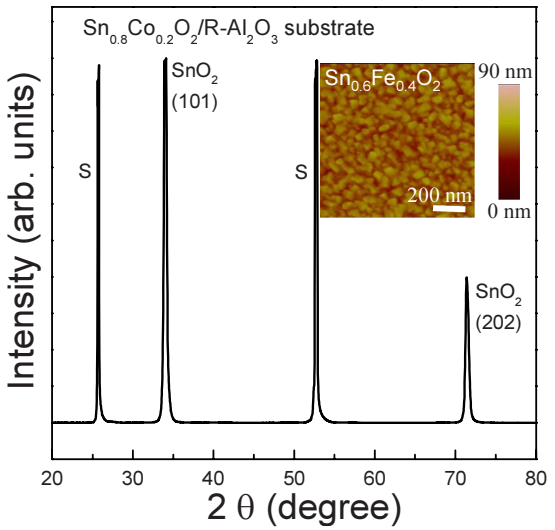

FIG. 1. (Color online) 1D XRD pattern of a $Sn_{0.8}Co_{0.2}O_2$ film grown on an *R*-plane Al_2O_3 substrate. "*S*" indicates substrate peaks. The inset shows an atomic force microscopy image of a 500-nm-thick $Sn_{0.6}Fe_{0.4}O_2$ film grown on an *R*-plane Al_2O_3 substrate. The scan area is 1×1 μm^2. The scale bar represents the height, spanning 90 nm differences between bright and dark regions.

parallel to the light propagation direction. The optical transmission measurements were performed within a wavelength range of 200–1750 nm using a Cary 5E UV-Vis-NIR dual-beam spectrophotometer.

III. EXPERIMENT RESULTS AND DISCUSSION

A. Structural properties

Figure 1 shows the 1D XRD pattern for a $Sn_{0.8}Co_{0.2}O_2$ film grown on *R*-plane $(1\bar{1}02)$ sapphire. The film consisted of (101) oriented single phase rutile structure without any detectable impurity phase such as Co, CoO, or Co_3O_4. For Fe-doped SnO_2 films, similar 1D XRD patterns were obtained for films with Fe concentration up to 40% (x=0.4) with no diffraction peaks from secondary phases. The inset of Fig. 1 shows an AFM image for a 500-nm-thick $Sn_{0.6}Fe_{0.4}O_2$ film, indicating a grain size of 40–100 nm and roughness below 5 nm. Figure 2(a) shows the 2D XRD pattern of the $Sn_{0.8}Co_{0.2}O_2$ film. The 2θ angle is equivalent to that of a conventional 1D θ-2θ scan while γ represents the out-of-plane tilt angle normal to the 2θ direction.[11] These data clearly show the epitaxial growth of the film. The bright spot represents diffraction planes in the single crystal, which have a well-defined value of 2θ and γ. The epitaxial growth of SnO_2 films is possible as a consequence of the structural match between Al_2O_3 and SnO_2 with a small misfit of −0.42% along $SnO_2[010]\|Al_2O_3[10\bar{1}0]$ and 11.52% along $SnO_2[10\bar{1}]\|Al_2O_3[\bar{1}\bar{2}31]$ in $SnO_2(101)\|Al_2O_3(1\bar{1}02)$.[12] As shown in Fig. 3, the cross-sectional HRTEM image indicates that the Co-doped SnO_2 film is epitaxially grown on the Al_2O_3 substrate and there is no segregation of secondary phases or structural inhomogeneity.

Figure 2(c) shows the *c*-axis lattice constants as a function of Co and Fe content. The *c*-axis dimension was deduced

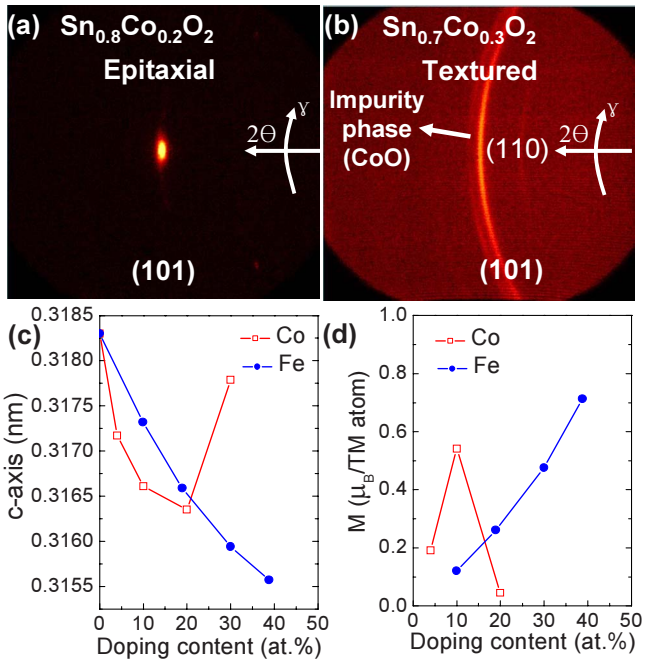

FIG. 2. (Color online) 2D XRD spectra of $Sn_{1-x}Co_xO_2$ films (a) with x=0.2 and (b) x=0.3. Co and Fe content dependence of (c) the lattice constant and (d) the magnetic moment.

from the measured d_{101} lattice spacing by assuming that the *a*-axis lattice constant of SnO_2 is the same as that of the Al_2O_3 substrate (0.4758 nm). The lattice constant decreases with increasing Co content, indicating solubility up to 20% Co concentration. Above 20% Co concentration, the lattice constant abruptly increases and an impurity phase, likely to be CoO, starts to appear, as evidenced by the 2D XRD pattern in Fig. 2(b), which also suggests a loss of epitaxy and a (101) textured growth for the film. In contrast, Fe ions can substitute for Sn ions up to 40 % concentration in a single phase material, as shown in Fig. 2(c). In the bulk, the solubility limit for both Co and Fe in SnO_2 is below 10 at %, and the high solubility of Co and Fe in the films is due to the nonequilibrium nature of the growth process in pulsed-laser deposition.[7] From the smaller out-of-plane lattice constant of

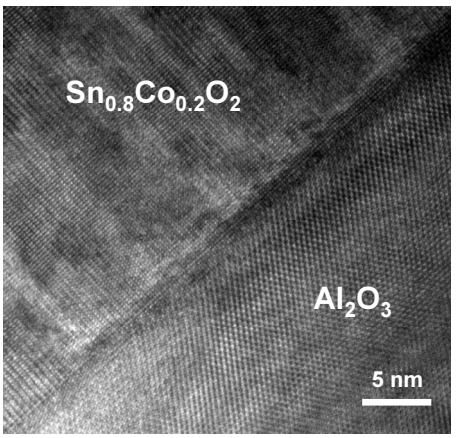

FIG. 3. The cross-sectional HRTEM image of $Sn_{0.8}Co_{0.2}O_2$ film.

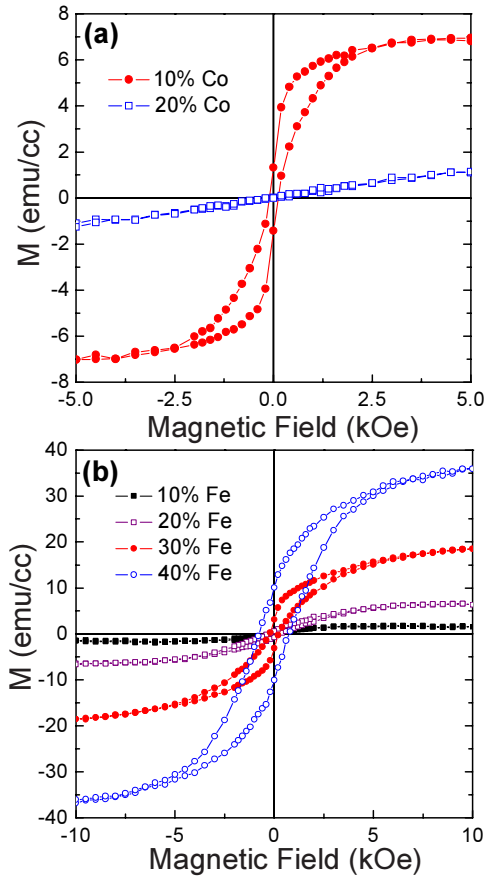

FIG. 4. (Color online) (a) Out-of-plane magnetization for $Sn_{1-x}Co_xO_2$ films with $x=0.1$ and 0.2 at 300 K. (b) Out-of-plane magnetization for $Sn_{1-x}Fe_xO_2$ films with $x=0.1$, 0.2, 0.3, and 0.4 at 300 K.

the films, as compared to that of bulk, we infer that the films grown on the Al_2O_3 substrate are under in-plane tensile strain.

B. Magnetic properties

We consider first the magnetization of the Co-doped films. A comparison of x-ray photoelectron spectroscopy binding energies of the Co primary and satellite XPS peaks in the films with that of Co^0 in Co metal, Co^{2+} in CoO, and Co^{3+} in Co_2O_3 (Refs. 13 and 14) shows that the oxidation state of Co in $Sn_{1-x}Co_xO_2$ films is Co^{2+}, and CoO or Co_3O_4 phases are not present. Figure 2(d) gives the magnetic moment of the films as a function of Co content, and Fig. 4(a) shows out-of-plane hysteresis loops at room temperature for the $Sn_{0.9}Co_{0.1}O_2$ and $Sn_{0.8}Co_{0.2}O_2$ films. The $Sn_{0.9}Co_{0.1}O_2$ film has a coercivity of 100 Oe and saturation moment of 0.54 μ_B/Co but the magnetic moment is considerably lower for $Sn_{0.8}Co_{0.2}O_2$. If Co^{2+} ions are in a high-spin state ($S=3/2$), the magnetic moment is 3 μ_B/Co while in the low-spin state ($S=1/2$), the moment is 1 μ_B/Co.[15] The measured film moments are smaller than either value. The decrease in moment for the higher Co content is consistent with antiferromagnetic Co^{2+}-O^{2-}-Co^{2+} superexchange pairings, as predicted by the Goodenough-Kanamori rules.[16,17] As x increases, the statistical fraction of unpaired Co, i.e., isolated Co sites, declines according to $(1-x)^z$, where z is the number of nearest-neighbor cations (six in the rutile structure). Evidence of decrease in effective moment per ion with increasing concentration was shown for Fe in In_2O_3.[9] The magnetic moment of the Co-doped SnO_2 lattice could therefore be accounted for by either-spin state of Co^{2+} or even by high-spin $Co^{3+}(S=2)$. Figure 5 shows the magnetization as a function of temperature for a $Sn_{0.9}Co_{0.1}O_2$ film measured from 10 to 1000 K. The SQUID data obtained for 10–300 K show that the saturation magnetization is almost constant over this temperature range. The magnetic moment of the film drops linearly above 300 K with an effective Curie temperature (T_C) of around 900 K, which makes it unlikely that ferromagnetic Co metal particles ($T_C \sim 1388$ K) (Ref. 18) contribute to the moment. This conclusion is supported further by the non-Brillouin contour of the descending thermomagnetism curve, which indicates the absence of a conventional ferromagnetic exchange field.

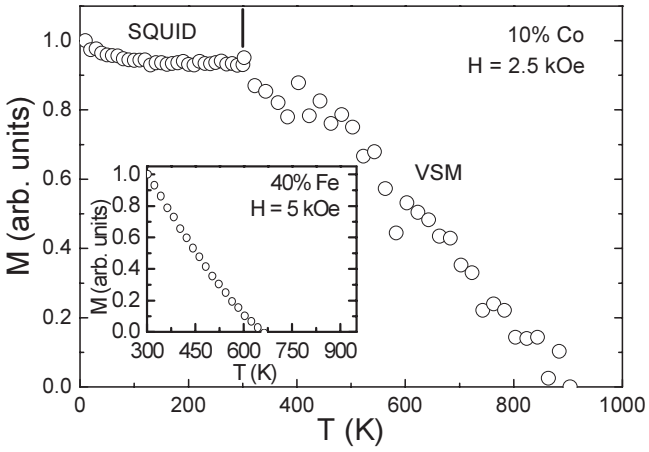

FIG. 5. The temperature dependence of saturation magnetization for the $Sn_{0.9}Co_{0.1}O_2$ film. $M(t)$ is normalized by magnetization at 10 K. The inset shows the temperature dependence of saturation magnetization for the $Sn_{0.6}Fe_{0.4}O_2$ film. $M(t)$ is normalized by magnetization at 300 K.

We now describe the behavior of Fe-doped SnO_2. Figures 2(d) and 4(b) show that the saturation moment at 10 kOe increases from 0.12 μ_B/Fe for $Sn_{0.9}Fe_{0.1}O_2$ to 0.71 μ_B/Fe for $Sn_{0.6}Fe_{0.4}O_2$ and the coercivity increases from 300 to 800 Oe. If ferromagnetic Fe_3O_4 were present, a comparison of the measured moments of 0.71 μ_B/Fe with that of Fe_3O_4 (1.3 μ_B/Fe) (Ref. 18) indicates that 55% of total Fe atoms in the film would need to be incorporated into Fe_3O_4 to obtain the measured magnetic moment and such a high percent of Fe in Fe_3O_4 would be detectable by XRD. The inset of Fig. 5 shows that the Curie temperature of the $Sn_{0.6}Fe_{0.4}O_2$ film was 650 K, which is similar to a value ($T_C \sim 610$ K) obtained by Coey *et al.* for 14% Fe in SnO_2,[6] and features a thermomagnetic characteristic similar to that of the 10% Co ions in the SnO_2 film.

XPS measurements reveal that the Fe is present as mixed valence Fe^{2+} and Fe^{3+} situated in the SnO_2 lattice. The presence of mixed valence enables both antiferromagnetic Fe^{3+}-O^{2-}-Fe^{3+} and Fe^{2+}-O^{2-}-Fe^{2+}, and ferromagnetic

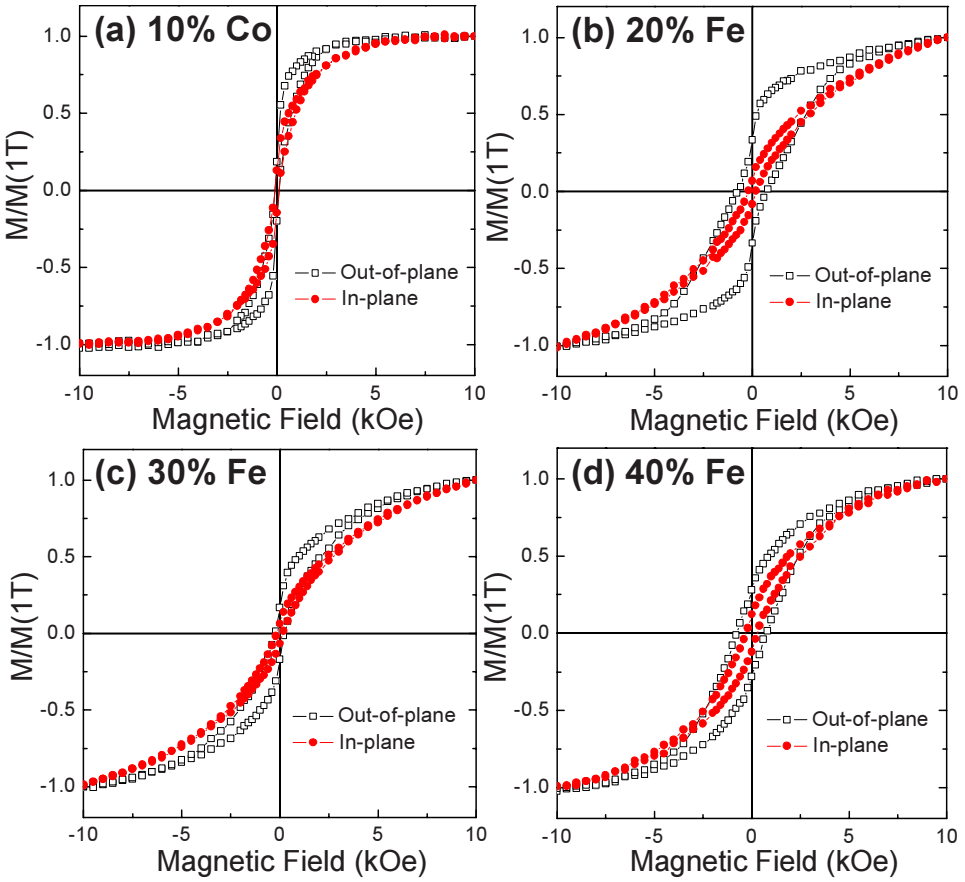

FIG. 6. (Color online) Hysteresis loops for (a) $Sn_{0.9}Co_{0.1}O_2$, (b) $Sn_{0.8}Fe_{0.2}O_2$, (c) $Sn_{0.7}Fe_{0.3}O_2$, and (d) $Sn_{0.6}Fe_{0.4}O_2$ films measured with field applied parallel and perpendicular to the film plane. $M(h)$ is normalized by magnetization at 1 T. In each case, an out-of-plane easy axis results from in-plane tensile stress, thereby confirming that the magnetostriction is negative (contraction), consistent with a Jahn-Teller splitting of the t_{2g} degenerate orbital states characteristic of Co^{2+}, Co^{3+}, and Fe^{2+} in octahedral sites (Refs. 9 and 10)

Fe^{3+}-O^{2-}-Fe^{2+} double-exchange-coupled pairs to be present in the material.[19] There is no evidence for impurity phase γ-Fe_2O_3 or Fe_3O_4.[20] As the number of Fe^{2+}-O^{2-}-Fe^{3+} pairings grows with x, ferromagnetism can become dominant through double exchange in the manner of Mn^{3+}-O^{2-}-Mn^{4+} couplings in mixed valence $La_{1-x}Ca_xMn^{3+}_{1-x}Mn^{4+}_xO_3$.[21]

C. Magnetoelastic properties

Figure 6(a) compares the hysteresis loops of a $Sn_{0.9}Co_{0.1}O_2$ film measured with field applied parallel and perpendicular to the film plane. An out-of-plane easy axis is apparent, which suggests that inverse magnetostriction effects in the strained film are responsible for the observed magnetic anisotropy.[8–10] Similar to Co-doped SnO_2, Fe-doped SnO_2 exhibits magnetic anisotropy with an out-of-plane easy axis [Figs. 6(b)–6(d)].

The anisotropy and magnetostriction in oxide lattices are attributed to TM ions, and originate from local orbit-lattice interactions, usually in an octahedral site. Where the orbital ground state of the cation is degenerate in cubic symmetry, the electronic structure in the crystal field can be stabilized further by an axial distortion (an isolated Jahn-Teller effect that produces a c-axis expansion with a doublet e_g ground state or a compression when it is a t_{2g} triplet), rendering the orbital angular momentum also sensitive to external stress. Spin-orbit coupling then influences the spin direction to select the c axis as either easy or hard in determining the magnetocrystalline anisotropy of the site.

In the Co-doped SnO_2 compounds, $Co^{3+}(3d^6)$ and $Co^{2+}(3d^7)$ would both qualify as magnetoelastic because of their t_{2g} ground states (assuming a complete six ligands). $Co^{4+}(3d^5)$ could also cause a c-axis compression but only in a low-spin $S=1/2$ configuration. All three valence states could cause the negative magnetostriction effects shown in the data of Fig. 6(a).

For Fe in SnO_2, a similar situation occurs but with different ionic charges. $Fe^{2+}(3d^6)$ or $Fe^{4+}(3d^4)$ would be magnetoelastic but only Fe^{2+} should produce the negative magnetostriction exhibited. The third ionic state $Fe^{3+}(3d^5)$, although likely present in significant amounts, is not magnetoelastic because of its orbital singlet ground state. In the progression of hysteresis loop shapes with increasing Fe content, the evolution begins with local behavior from ions in isolated sites with a pronounced easy axis normal to the film plane, and evolves into a "soft knee" loop with remanence and high coercivity. As the Fe concentration increases to $x=0.4$, room-temperature magnetization follows a slower approach to saturation, masking to some extent the out-of-plane easy axis by the appearance of an offsetting shape demagnetizing field. At this higher concentration, ferromagnetism can occur by short-range charge transfer $Fe^{2+} \leftrightarrow Fe^{3+}+e^-$ (double exchange). Trivalent Fe is not magnetoelastic to first order; however, if there is enough present to produce a saturation magnetization $4\pi M_s \sim 1$ kG, not only will the demagnetization effect soften the knee of loop but the anisotropy may now contribute to domain-wall energies that result in the 800 Oe coercivity and a measurable remanence.

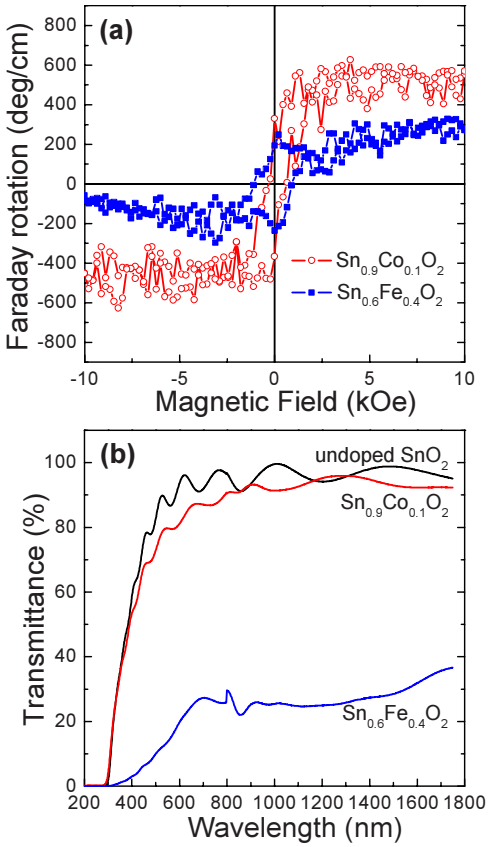

FIG. 7. (Color online) (a) Faraday rotation of $Sn_{0.9}Co_{0.1}O_2$ and $Sn_{0.6}Fe_{0.4}O_2$ films at 1550 nm wavelength, as a function of magnetic field applied perpendicular to the film plane. (b) Optical transmission spectra of undoped SnO_2 $Sn_{0.9}Co_{0.1}O_2$, and $Sn_{0.6}Fe_{0.4}O_2$ films.

As a comparison with the epitaxial films, we found that Co- and Fe-doped SnO_2 films grown on Si substrates, where the films are polycrystalline and not heavily strained, do not show any magnetic anisotropy.

D. Magneto-optical properties

Figure 7(a) shows the Faraday rotation of $Sn_{0.9}Co_{0.1}O_2$ and $Sn_{0.6}Fe_{0.4}O_2$ films at 1550 nm wavelength as a function of applied magnetic field, measured with the magnetic field perpendicular to the film plane. The Faraday rotation hysteresis loop may be compared with the out-of-plane hysteresis loop obtained by VSM. We note some discrepancy between the Faraday and magnetic loops, for example, the coercivities differ. The magnetic hysteresis loop can be explained classically in terms of rotating magnetization vectors in a magnetic field where the only quantum state involved is the ground state. On the other hand, the magneto-optical loop involves an excited state that is largely uncharacterized. The selection rules are $\Delta L_z=1$ and $\Delta S_z=0$.[22] It could be that the excited state has the controlling influence in the magneto-optical loop.

The saturation Faraday rotation of $Sn_{0.9}Co_{0.1}O_2$ and $Sn_{0.6}Fe_{0.4}O_2$ films was 570°/cm and 280°/cm, respectively. The limited Faraday rotation of these materials can be explained by high birefringence due to the highly anisotropic refractive index in the tetragonal rutile structure of SnO_2. Thin-film linear birefringence (the difference between the refractive indices of the transverse electric and transverse magnetic modes) significantly limits the resultant Faraday rotation to spatially periodic oscillations between small positive and negative angles.[23,24] XRD analysis has confirmed that the deviation from a cubic structure, defined as the ratio of the c-lattice constant to the a-lattice constant, was 0.6654 and 0.6632 for $Sn_{0.9}Co_{0.1}O_2$ and $Sn_{0.6}Feo_{0.4}O_2$ films, respectively. As a comparison, the c/a ratio for bulk SnO_2 is 0.6726.[25] To reduce the birefringence effects, patterning of the material into optical waveguides, as has been demonstrated in garnet films,[26] is currently in progress.

The optical transmission spectra for undoped SnO_2, $Sn_{0.9}Co_{0.1}O_2$, and $Sn_{0.6}Fe_{0.4}O_2$ films are shown in Fig. 7(b). By observing the decrease of the transmission intensity and the reduction of the interference fringes, it is apparent that the material becomes increasingly opaque as the Co and Fe doping level increases. Due to the high transparency of the Al_2O_3 substrate at infrared wavelength, we applied the method of Ref. 27 to calculate the refractive index (n) and extinction coefficient (k) of undoped SnO_2 and $Sn_{0.9}Co_{0.1}O_2$ at 1550 nm wavelength. The undoped SnO_2 film has $n=1.949$ and $k=0.0034$. The calculated refractive index for undoped SnO_2 agrees very well with the reported value in Ref. 28. $Sn_{0.9}Co_{0.1}O_2$ has $n=1.957$ and $k=0.0102$. Calculation on the $Sn_{0.6}Feo_{0.4}O_2$ data was not carried out because very few interference fringes appear in the transmission spectra, rendering the calculation inaccurate. The relatively large absorption in $Sn_{1-x}Fe_xO_2$ film may be the result of mixed valence Fe^{2+}/Fe^{3+}, which is beneficial to ferromagnetism but detrimental to the optical transmission.[29]

The magneto-optical figure of merit, which is the ratio of the Faraday rotation to optical loss, is 0.16°/dB at 1550 nm for $Sn_{0.9}Co_{0.1}O_2$. As a comparison, values of 25.8°/dB and 9.1°/dB have been reported for single-crystal garnets of composition $Yb_{0.25}Bi_{0.46}Y_{2.29}Fe_5O_{12}$ and $Y_3Fe_5O_{12}$ at the same wavelength, respectively.[30] $Sn_{0.9}Co_{0.1}O_2$ film may be useful in devices based on nonreciprocal phase shift,[31] which are less sensitive to birefringence.

Without measurement data across the spectral band of interest, it is difficult to identify the electric-dipole transitions responsible for the Faraday rotation effect. The absorption-line center could be near the 1550 nm wavelength of interest if the line oscillator strength is weak or far from it if the strength is high. Moreover, there is insufficient information to decide whether the transition is paramagnetic or diamagnetic. Both Co and Fe have spectral lines that could produce the results in Fig. 7. If there are few "non-Faraday" transitions near the signal wavelength, the figure of merit can help somewhat as a guide: Low figure of merit suggests proximity to a Lorentzian line center, which might be the case here. Therefore, the source would more likely be from paramagnetic ground states within the crystal-field energy regime (<1 eV), which points to Co^{2+} and Fe^{3+} in octahedral sites.[32]

E. Anomalous Hall effect

The magnetic-field dependence of the Hall resistance (R_H) for a $Sn_{0.6}Fe_{0.4}O_2$ film and a $Sn_{0.9}Fe_{0.1}O_2$ film is shown in

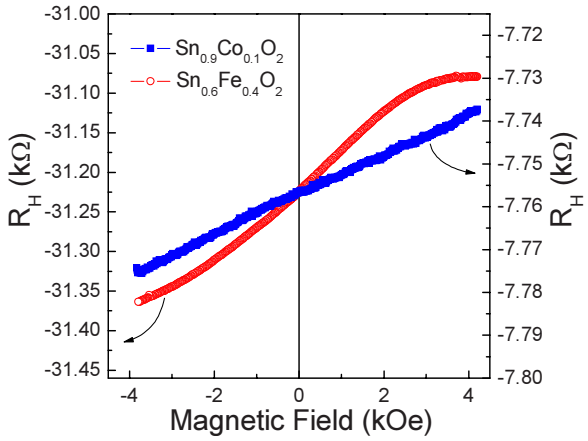

FIG. 8. (Color online) Magnetic-field dependence of Hall resistance (R_H) for $Sn_{0.9}Co_{0.1}O_2$ and $Sn_{0.6}Fe_{0.4}O_2$ films.

Fig. 8. The Hall resistance of the $Sn_{0.6}Fe_{0.4}O_2$ exhibits a nonlinear, anomalous behavior, indicating the presence of interactions between itinerant carriers and the localized spins of the Fe ions,[8] i.e., a form of double exchange. In previous work, TM-doped SnO_2 has not shown an anomalous Hall effect (AHE) so it has been proposed that localized ferromagnetic exchange in doped SnO_2 is instead caused by spin-polarized electrons "trapped" in oxygen vacancies.[6,33]

Substitution of Sn^{4+} by TM^{2+}/TM^{3+} requires defects for charge compensation. In view of the high levels of TM ions that can be incorporated in SnO_2, the charge-compensating defects are likely to be electronic in nature, e.g., holes, rather than interstitials (Sn^{2+}) or oxygen vacancies, which would destabilize the rutile structure if present at high concentration. Such defects could be depicted as *p*-type peroxide sites created by local $Fe^{4+}+2O^{2-}\rightarrow Fe^{3+}+O^{2-}+O^{-}\rightarrow Fe^{2+}+2O^{-}$ charge-transfer reactions. Our $Sn_{0.6}Fe_{0.4}O_2$ film indeed has a *p*-type carrier concentration of 5×10^{18} cm^{-3}. This is low in comparison to the undoped SnO_2 film, which exhibits *n*-type carrier concentration of 2×10^{19} cm^{-3}. This can be interpreted as due to the charge compensation arising as a result of hole doping by Fe incorporation into the lattice. The *p*-type conduction of our samples is fundamentally different from the *n* type observed in Mn-doped SnO_2:Sb,[7] which is due to the Sb donors.

In contrast, AHE was not observed in a $Sn_{0.9}Co_{0.1}O_2$ film, which has a higher *p*-type carrier concentration of 1.5×10^{19} cm^{-3} than the $Sn_{0.6}Fe_{0.4}O_2$ film. This suggests that the ferromagnetism in Co- and Fe-doped SnO_2 is not carrier mediated, and the RKKY (Ruderman-Kittel-Kasuya-Yosida)-type interactions based on *sp-d* exchange between TM ions and free carriers are unlikely.[34,35] Recently, Griffin *et al.* have reported intrinsic room-temperature ferromagnetism in highly insulating Co-doped TiO_2 films.[15] They concluded that free carriers, which interact with the localized magnetic moment of TM ions, are not required for ferromagnetic ordering in TM-doped oxides. Also, it should be noted that AHE is not always a good indicator of intrinsic ferromagnetism, as AHE was observed in Co-doped TiO_2 films with Co metal clusters.[36]

IV. SUMMARY AND CONCLUSIONS

Epitaxial films of magnetically doped rutile-structure tin oxide, $Sn_{1-x}Co_xO_2$ ($x\leq0.2$) and $Sn_{1-x}Fe_xO_2$($x\leq0.4$), were grown on *R*-Al_2O_3 substrates by PLD. Films have an out-of-plane magnetic anisotropy and magnetization of up to 0.54 μ_B/Co atom (at $x=0.1$) and 0.71 μ_B/Fe atom (at $x=0.4$).

Based on the measurement data presented in the foregoing sections, we can conclude that substantial fractions of the Co and Fe in $Sn^{4+}O_2$ have valence states below 4+. Charge compensation is accomplished by oxygen vacancies as well as the likely excitation of *p*-type carriers (holes) in the *O* band. The high magnetic anisotropy observed in Co- and Fe-doped SnO_2 films is consistent with the presence of substantial amounts of magnetoelastic high-spin Fe^{2+} and either-spin Co^{2+}. Our AHE study showed that room-temperature ferromagnetism in Co- and Fe-doped SnO_2 films is not carrier mediated.

There would only be significant fractions of cations isolated as paramagnetic sites when $x<0.2$. Despite this fact, however, the peculiarities of the DMS systems continue to exist at higher concentrations—high magnetoelasticity and high effective Curie temperature[9]—with the same local spin-orbit-lattice couplings regardless of the presence, absence, or magnitude of a conventional ferromagnetic exchange field. Therefore, magnetoelastic effects from TM ions contribute to magnetic hysteresis and thermomagnetism, and based on energy stabilization requirements, could be necessary conditions for dilute magnetic ordering above room temperature.

The deviation of rutile-structured SnO_2 from uniaxial symmetry leads to significant birefringence and therefore limits the Faraday rotation achievable in these materials. $Sn_{0.9}Co_{0.1}O_2$ has a Faraday rotation of 570°/cm accompanied by optical losses of $k=0.0102$, which makes it an interesting candidate for thin-film magneto-optical applications.

ACKNOWLEDGMENTS

The authors would like to acknowledge F. J. Castaño for useful discussions and YoungJu Park for Hall measurements. This work was supported by Korea Research Foundation Grant funded by the Korean Government (MOEHRD) (Grant No. KRF-2006–352–D00094) and by the National Science Foundation, Division of Materials Research.

*Present Address: Lincoln Laboratory, Massachusetts Institute of Technology, Lexington, Massachusetts 02420, USA.
†caross@mit.edu

[1] G. A. Prinz, Science **282**, 1660 (1998).
[2] H. Ohno, A. Shen, F. Matsukura, A. Oiwa, A. Endo, S. Katsumoto, and Y. Iye, Appl. Phys. Lett. **69**, 363 (1996).
[3] T. Dietl, J. Appl. Phys. **89**, 7437 (2001).
[4] V. Zayets, M. C. Debnath, and K. Ando, Appl. Phys. Lett. **84**, 565 (2004).
[5] S. B. Ogale, R. J. Choudhary, J. P. Buban, S. E. Lofland, S. R. Shinde, S. N. Kale, V. N. Kulkarni, J. Higgins, C. Lanci, J. R. Simpson, N. D. Browning, S. Das Sarma, H. D. Drew, R. L. Greene, and T. Venkatesan, Phys. Rev. Lett. **91**, 077205 (2003).
[6] J. M. D. Coey, A. P. Douvalis, C. B. Fitzgerald, and M. Venkatesan, Appl. Phys. Lett. **84**, 1332 (2004).
[7] H. Kimura, T. Fukumura, M. Kawasaki, K. Inaba, T. Hasagawa, and H. Koinuma, Appl. Phys. Lett. **80**, 94 (2002).
[8] J. Philip, A. Punnoose, B. I. Kim, K. M. Reddy, S. Layne, J. O. Holmes, B. Satpati, P. R. Leclair, T. S. Santos, and J. S. Moodera, Nat. Mater. **5**, 298 (2006).
[9] G. F. Dionne, J. Appl. Phys. **101**, 09C509 (2007).
[10] G. F. Dionne and H. S. Kim, J. Appl. Phys. **103**, 07B333 (2008).
[11] B. B. He, U. Preckwinkel, and K. L. Smith, Adv. X-Ray Anal. **43**, 273 (2000).
[12] J. Lu, J. Sundqvist, M. Ottosson, A. Tarre, A. Rosental, J. Aarik, and A. Harsta, J. Cryst. Growth **260**, 191 (2004).
[13] S. A. Chambers, R. F. C. Farrow, S. Maat, M. F. Tonney, L. Folks, J. G. Catalano, T. P. Trainor, and G. E. Brown, Jr., J. Magn. Magn. Mater. **246**, 124 (2002).
[14] J. F. Moulder, W. F. Stickle, P. E. Sobol, and K. D. Bomben, *Handbook of X-Ray Photoelectron Spectroscopy* (Perkin-Elmer, Eden Prairie, MN, 1992).
[15] K. A. Griffin, A. B. Pakhomov, C. M. Wang, S. M. Heald, and K. M. Krishnan, Phys. Rev. Lett. **94**, 157204 (2005).
[16] J. B. Goodenough, *Magnetism and the Chemical Bond* (Wiley, New York, 1963), Chap. III.
[17] J. Kanamori, J. Phys. Chem. Solids **10**, 87 (1959).
[18] R. C. O'Handley, *Modern Magnetic Materials: Principles and Applications* (Wiley, New York, 2000).
[19] G. F. Dionne, in *Magnetic Interactions and Spin Transport*, edited by A. Chtchelkanova, S. A. Wolf, and Y. Idzerda (Springer, New York, 2003), Chap. 1.
[20] N. S. Mcintyre and D. G. Zetaruk, Anal. Chem. **49**, 1521 (1977).
[21] G. F. Dionne, J. Appl. Phys. **79**, 5172 (1996).
[22] G. F. Dionne, A. R. Taussig, M. Bolduc, L. Bi, and C. A. Ross, J. Appl. Phys. **101**, 09C524 (2007).
[23] R. Wolfe, V. J. Fratello, and M. McGlashan-Powell, Appl. Phys. Lett. **51**, 1221 (1987).
[24] A. R. Taussig, G. F. Dionne, and C. A. Ross, Phys. Rev. B **77**, 012407 (2008).
[25] JCPDS Card No. 41-1445 (unpublished).
[26] H. Dötsch, N. Bahlmannm, O. Zhuromskyy, M. Hammer, L. Wilkens, R. Gerhardt, and P. Hertel, J. Opt. Soc. Am. B **22**, 240 (2005).
[27] R. Swanepoel, J. Phys. E **16**, 1214 (1983).
[28] J. Schoenes, U. Pelzer, D. Menzel, K. Franke, F. Ludwig, and M. Schilling, Phys. Status Solidi C **3**, 4115 (2006).
[29] T. Tepper, G. F. Dionne, and C. A. Ross, IEEE Trans. Magn. **40**, 1685 (2004).
[30] W. Zhao, Sens. Actuators, A **89**, 250 (2001).
[31] J. Fujita, M. Levy, R. U. Ahmad, R. M. Osgood, Jr., M. Randles, C. Gutierrez, and R. Villareal, Appl. Phys. Lett. **75**, 998 (1999).
[32] D. S. McClure, Solid State Phys. **9**, 399 (1959).
[33] J. M. D. Coey, M. Venkatesan, and C. B. Fitzgerald, Nat. Mater. **4**, 173 (2005).
[34] T. Dietl, H. Ohno, F. Matsukura, J. Cibert, and D. Ferrand, Science **287**, 1019 (2000).
[35] J. König, H. H. Lin, and A. H. MacDonald, Phys. Rev. Lett. **84**, 5628 (2000).
[36] S. R. Shinde, S. B. Ogale, J. S. Higgins, H. Zheng, A. J. Millis, V. N. Kulkarni, R. Ramesh, R. L. Greene, and T. Venkatesan, Phys. Rev. Lett. **92**, 166601 (2004).